Journal of the Meteorological Society of Japan, Vol. 89, No. 5, pp. 475–493, 2011
DOI:10.2151/jmsj.2011-505

Hadley and Walker Circulations in the Mid-Pliocene Warm Period Simulated by an Atmospheric General Circulation Model

Youichi KAMAE, Hiroaki UEDA

Graduate School of Life and Environmental Sciences University of Tsukuba, Tsukuba, Japan

and

Akio KITOH

Meteorological Research Institute, Tsukuba, Japan

(Manuscript received 22 November 2010, in final form 6 June 2011)

Abstract

The mid-Pliocene warm period (∼3 million years ago; 3 Ma) is one of the plausible scenarios which provide insight into the climate system in a globally warmer world as projected by climate models for the future. The reconstructed sea surface temperature (SST) by the Pliocene Research, Interpretation and Synoptic Mapping phase 3 (PRISM3) reveals that salient warming occurs in the higher latitudes together with weakening of surface cooling in the equatorial and coastal upwelling regions. The sensitivity of an atmospheric general circulation model (AGCM) is studied by prescribing the surface condition based on the PRISM3 paleoenvironmental reconstructions. The simulated Walker circulation generally slows down, inducing convergent anomaly over the African continent and divergent anomaly over the Asian monsoon region at the lower troposphere; and vice versa at the upper troposphere in response to the reduced east-west gradient of the tropical SST in that period. The ascending branch of the Hadley cell expands poleward, implying a weakening of the meridional circulation in response to the warmer SST in the higher latitudes. To identify the physical reason for the modulation of the wet-dry climatological pattern in low latitudes, additional sensitivity experiments were conducted by changing the configurations of ice-sheet cover, vegetation and zonal patterns of the SST. The results indicate that the reduction of meridional and zonal gradient of tropical SST is the key factor for the expansion of proxy-suggested wetter climate over Africa.

1. Introduction

The mid-Pliocene warm period (∼3 million years ago; 3 Ma) is a warm interval experienced in transition from the sustained warmer climate of the early Pliocene , with relatively small (or absent) Northern Hemisphere ice sheets, to the cooler climate of the Quaternary, with predominant glacial-interglacial cycles (e.g., Zachos et al. 2001; Lisiecki and Raymo 2005; Jansen et al. 2007). It is also the most recent period when the global climate was substantially warmer than the present-day for a sustained time (∼300 thousand years, e.g., Dowsett et al. 1994; Haywood et al. 2009a). In addition, the geographic distribution of continents and oceans in this period was similar to that in the present day. The effort in simulating the climate for this interval is expected to make substantial contributions to the advanced validation of climate models predicting future climate change (e.g., Crowley 1996; Salzmann et al. 2009), to the esti-

Corresponding author: Youichi Kamae, Graduate School of Life and Environmental Sciences, University of Tsukuba, 1-1-1 Tennoudai Tsukuba-shi, Ibaraki 305-8572, Japan
E-mail: s0930225@u.tsukuba.ac.jp

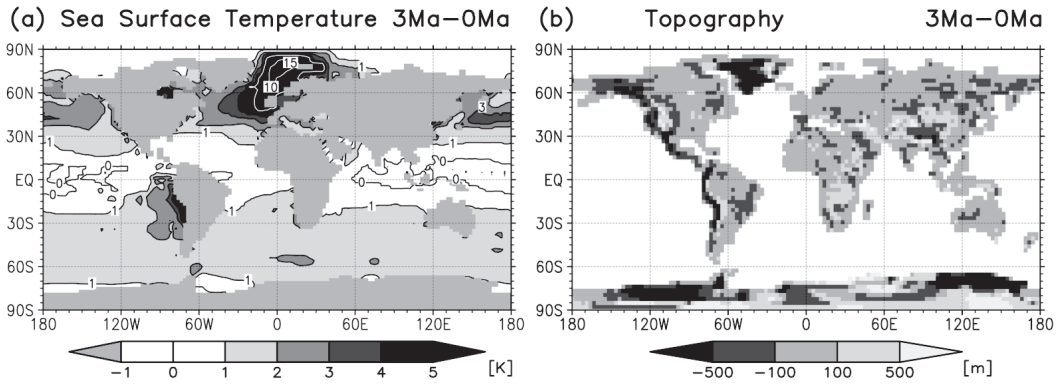

Fig. 1. Differences in boundary conditions used in the AGCM (3 Ma minus 0 Ma). (a) Annual mean SST (K). Black and white contour interval is 1, 5 K, respectively. (b) Topography (m).

mation of "Earth system sensitivity" (Lunt et al. 2010; Pagani et al. 2010), and to provide insight into the globally warmer world that is predicted by the climate models for the future(e.g., Meehl et al. 2007; Knutti and Hegerl 2008).

The paleoclimate conditions in the mid-Pliocene are investigated by a series of studies that summarized conditions at a large number of marine and terrestrial sites and areas. As a part of the United State Geological Survey (USGS) Global Changes Research effort, the Pliocene Research Interpretation and Synoptic Mapping (PRISM) Project (e.g., Dowsett et al. 1994, 1996, 1999, 2009b) has documented the characteristics of climate in the mid-Pliocene warm period (3.29–2.97 Ma) on a global scale by use of various types of proxy records (e.g., foraminifera, diatoms, ostracods, pollen and plant macrofossil data). The PRISM datasets have been used to drive numerical simulations designed to explore the impact of climate forcing and feedback during the Pliocene (e.g., Chandler et al. 1994; Sloan et al. 1996; Jiang et al. 2005), and assess the reproducibility of climate simulations derived by general circulation models (GCMs) in this period (e.g., Haywood et al. 2005; Haywood et al. 2009b). Recently, as a worldwide framework for studying the paleoclimate reconstructions and simulations, the Paleoclimate Modeling Intercomparison Project (PMIP; e.g., Joussaume et al. 1999; Braconnot et al. 2007a, b) has focused on the mid-Pliocene warm period as one of new target intervals in its latest phase (PMIP3; Otto-Bliesner et al. 2009).

Figure 1 shows sea surface temperature (SST) and topography in the mid-Pliocene warm period reconstructed by the latest phase of the PRISM project (PRISM3; Haywood et al. 2010). The SST reconstruction (Fig. 1a) features pronounced warming (up to $\sim$15 K) in mid- and high-latitudes, particularly in the North Atlantic Ocean (e.g., Dowsett et al. 1996). In contrast, the SST is similar to the present day value in tropical regions. The SST pattern in the mid-Pliocene is distinct from the significant warming trend in low latitude in the future projection by experiments forced by increasing atmospheric greenhouse gases concentrations (e.g., Meehl et al. 2007). Recently, it was revealed that the proxy records from the modern upwelling areas off the west coast of South America suggest warmer surface conditions in the mid-Pliocene than the present day (e.g., Ravelo et al. 2004; Haywood et al. 2005; Wara et al. 2005; Dekens et al. 2007; Dowsett and Robinson 2009). The east-west anomalous SST contrast in the tropics (Fig. 1a) could have played a fundamental role for atmospheric general circulation patterns and global climate in the mid-Pliocene (e.g., Etourneau et al. 2010; Ravelo 2010).

Numerical studies through the use of GCMs evoked some features of the atmospheric general circulation in the mid-Pliocene. One of the key aspects of the mid-Pliocene climate was a weakening of atmospheric east-west overturning circulation in the tropics, manifested as Walker circulation, as a part of a "permanent El-Niño" condition (e.g., Barreiro et al. 2006; Brierley et al. 2009) resulting from the reduction of east-west temperature gradient in the tropical Pacific (e.g., Ravelo et al. 2004; Wara et al. 2005; Dekens et al. 2007). As for the latitudinal direction, characteristics of mean meridional circulation (MMC) in the tropics (Hadley circulation) during this interval were investigated by various configurations (Sloan et al. 1996; Barreiro et al. 2006). The AGCM studies forced by SST with coarser reso-

lution or present-day meridional gradient in the tropics did not show any significant changes in the strength and location of the Hadley circulation. In contrast, weakening of the Hadley circulation has been also reported in several studies (e.g., Chandler et al. 1994; Haywood et al. 2000; Jiang et al. 2005). Brierley et al. (2009) revealed that a diminished meridional gradient of SST in low latitude, as based on several types of proxy records, is responsible for the greatly weakened and a latitudinal expansion of the Hadley circulation in early Pliocene (ca. 4 Ma). Haywood et al. (2009b) showed broadening of the Hadley cells caused by reduction in the equator-to-pole temperature gradient in the results of two AGCM simulations using PRISM2 boundary conditions (Dowsett et al. 1999).

In addition to the alteration of the high-latitude climate, the reconstructed air temperature and rainfall show that the atmospheric circulation in low latitude was also largely modulated, and inherent physical processed are insufficiently understood, especially monsoon related wet/dry climate (e.g., Chandler et al. 1994; Sloan et al. 1996; Haywood et al. 2009b). The improvement in the reconstruction of the paleoenvironmental conditions by PRISM has provided insight into large-scale atmospheric circulation for altered regional climate patterns under warmer conditions as well as validation of the simulation with paleovegetation data. The purpose of the present study is examining the details of atmospheric global circulation and tropical/subtropical climate patterns in low latitude during the mid-Pliocene warm period by use of state-of-the-art PRISM reconstruction dataset, which has additional data points in equatorial Pacific and other regions. Examining the consistency of simulated climate with the terrestrial proxy data may contribute to test the ability of GCM to simulate the climate under the warmer conditions. It should be noted that formation of the climate system through the modulation of the oceanic general circulation and SST distribution during this period is not discussed in this study because sea surface conditions, which also includes substantial influences over the other boundary conditions, are prescribed. We only consider the annual-mean values in this paper because the information about seasonality in proxy data was not sufficient to verify the results of simulations. The paper is organized as follows: Section 2 describes the atmospheric GCM, boundary conditions, experimental design, and analysis method. Section 3 represents the characteristics of simulated atmospheric circulation in the mid-Pliocene and discusses possible mechanisms for the climate changes in the mid-Pliocene. Section 4 is discussion. Section 5 is the conclusion of this paper.

2. Data and method

2.1 Atmospheric general circulation model (AGCM)

The model used for the present study is an atmospheric component of an air-sea coupled model developed at the Meteorological Research Institute in Japan (MRI-CGCM2.3; Yukimoto et al. 2001, 2006) for climate projections and paleoclimate simulations (e.g., Kitoh et al. 2001; Kitoh and Murakami 2002; Ueda et al. 2011). The AGCM has horizontal T42 resolution (an approximately 280 km transform grid) and 30 layers in the vertical, with the top at 0.4 hPa. The land component is based on the simple biosphere (SiB) model (Sellers et al. 1986; Sato et al. 1989), which includes the effects of vegetation. The land model has three soil layers with different field capacities depending on the vegetation type, in which the temperature, liquid water, and frozen water in each soil layer are predicted. Canopy and grass are treated for each of the 13 vegetation types, for which the parameters are dependent on the vegetation type and month of the year.

2.2 Boundary conditions

The mid-Pliocene surface conditions used in this study are PRISM3 dataset (Haywood et al. 2010), which combines 202 terrestrial and 86 marine sites. This dataset is provided to the paleoclimate modeling community through a series of digital datasets as part of the PRISM data-model cooperative, also known as the Pliocene Model Intercomparison Project (PlioMIP). The PRISM3 paleoclimate reconstruction contains all major boundary conditions, including SST (Fig. 1a) and sea ice extent (Dowsett et al. 2009b; Haywood et al. 2010), ice sheet height and extent, vegetation types and distribution (Salzmann et al. 2008), and topography (Sohl et al. 2009).

Figure 1b shows differences in topography and ice sheet height between 3 Ma and the present day. The reconstruction of topography by palaeobotanical and palaeoelevation evidence shows that the East African Rift Valley was 500 m higher in the mid-Pliocene relative to the present value (Thompson and Fleming 1996; Dowsett et al. 1999; Sohl et al. 2009). In contrast, the western cordilleras of North America and northern South America were lower than the present day. Figure 2 shows the land ice distribution estimated by stable isotopic, stratigraphic sea level records, and pollen data on the land. This evidence reveals significant reduction of the continental ice sheet on Greenland and Antarctica (Thompson and Fleming 1996; Dowsett et al. 1999). The land ice extent over Greenland was reduced by half (Dowsett et al. 1999), with the ice restricted to the high

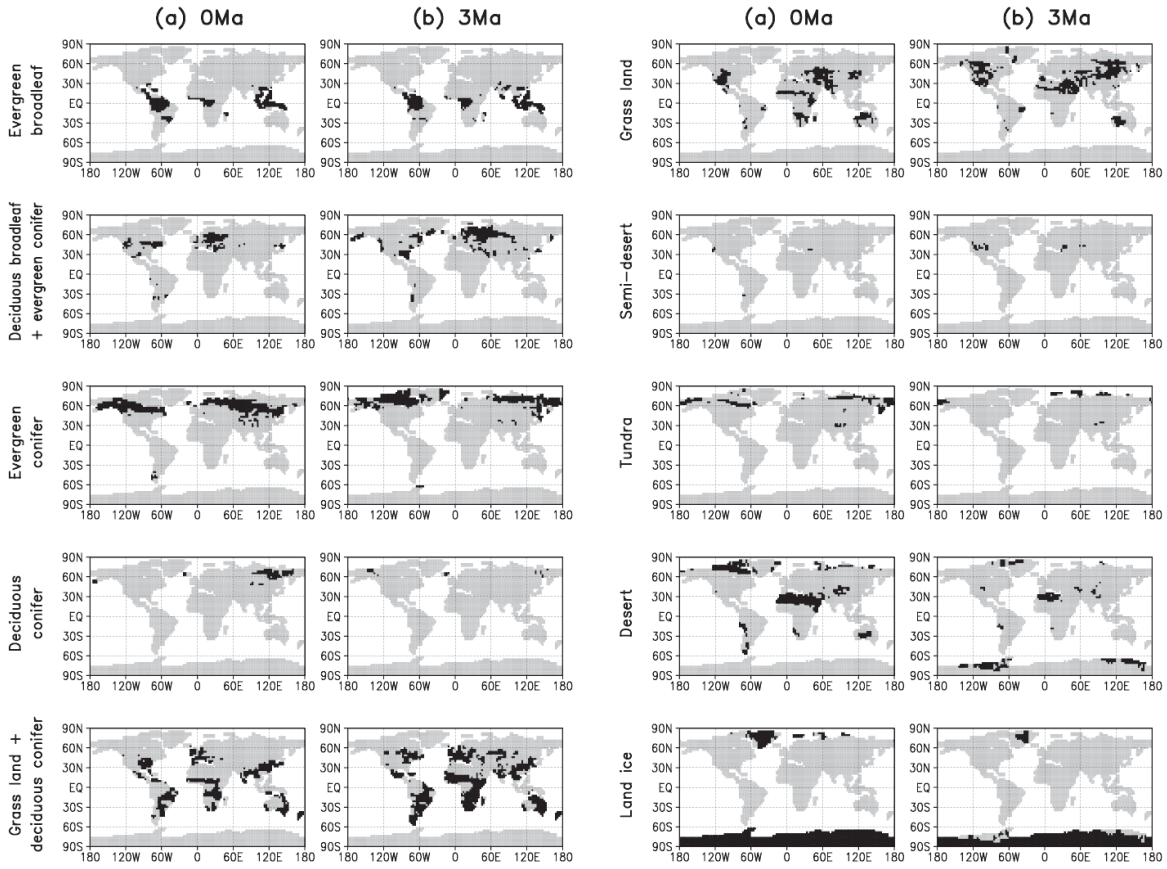

Fig. 2. Distributions of vegetation used in the AGCM, (a) 0 Ma, (b) 3 Ma. Vegetation type in each grid is classified into 13 types of SiB classification. None of the grids is classified into the three types of vegetation (deciduous broadleaf, broadleaf deciduous shrubs, cultivated land) in this study.

altitude regions of East Greenland. In East Antarctica, significant ice sheet reduction was recognizable in the Wilkes and Aurora Subglacial basins (Haywood et al. 2010).

Reconstruction of vegetation is compiled from fossil pollen and plant macrofossil data from terrestrial sites covering all continents (Thompson and Fleming 1996; Dowsett et al. 1999). The patterns of reconstructed vegetation in the mid-Pliocene (Fig. 2) indicate a generally warmer and moister climate relative to the present day. The major differences in vegetation patterns between the modern and the mid-Pliocene are significant reductions of tundra area accompanied by northward migration of evergreen taiga. The vegetation distribution was characterized by a parallel northward shift of temperate forests and grasslands in Eurasian and eastern North America, replacing the boreal conifer forests. In the lower latitude, the mixed warm-temperate forests in East Asia and North America became dominant in central Europe. The northward shift of vegetation patterns in mid- and high-latitude, together with significant reduction of continental ice sheet in Greenland and Antarctica suggests vastly warmer conditions than the present day, particularly at the polar regions (e.g., Salzmann et al. 2008). It is also notable that more humid conditions spread over broader areas in low latitude. Salzmann et al. (2008) revealed a wetter climate in the subtropics relative to the present day due to the expansion of tropical savannas and woodlands in Africa and Australia in the current expense of subtropical deserts.

PRISM3 SST differs from PRISM2 SST (Dowsett et al. 1999) by taking into account data from more localities, particularly in the equatorial Pacific (Dowsett and Robinson 2009) and North-eastern Atlantic/Arctic regions (Dowsett et al. 2009a, b; Robinson 2009). In addition, PRISM3 incorporates multiple tempera-

Table 1. External forcings and atmospheric constituents in this study.

Solar constant [W m^{-2}]	Eccentricity	Obliquity [°]	Precession [°]	CO_2 (0 Ma) [ppmv]	CO_2 (3 Ma) [ppmv]	CH_4 [ppbv]	N_2O [ppbv]
1365	0.016724	23.446	102.04	280	405	760	270

Table 2. Surface properties for the experiments. Spatial range where difference in topography and vegetation exists between 3 Ma and 0 Ma is entire region except Greenland and the Antarctic Continent. Differences of "Land ice" in orography and biomes between 3 Ma and 0 Ma exist only on the Greenland and Antarctic Continent.

Experiments	SST	Sea ice	Topography*	Land ice**	Vegetation*
0 Ma	**0 Ma**	**0 Ma**	**0 Ma**	**0 Ma**	**0 Ma**
3 Ma	3 Ma	3 Ma	3 Ma	3 Ma	3 Ma
3 Ma_0SST	**0 Ma**	3 Ma	3 Ma	3 Ma	3 Ma
3 Ma_0Sea ice	3 Ma	**0 Ma**	3 Ma	3 Ma	3 Ma
3 Ma_0Topo	3 Ma	3 Ma	**0 Ma**	3 Ma	3 Ma
3 Ma_0Land ice	3 Ma	3 Ma	3 Ma	**0 Ma**	3 Ma
3 Ma 0Veg	3 Ma	3 Ma	3 Ma	3 Ma	**0 Ma**

*except the Greenland and the Antarctic Continent

**only on the Greenland and the Antarctic Continent

Table 3. SST configurations in the idealized experiments. The other boundary conditions in the experiments are similar to the 3 Ma simulation. The configurations in the two contrast experiments are shown in the upper column.

Experiments	SST in the Pacific Ocean and the Indian Ocean	SST in the Atlantic Ocean and the Arctic Ocean
3 Ma	3 Ma	3 Ma
3 Ma_0SST	0 Ma	0 Ma
3 Ma_ZSST	3 Ma zonal	3 Ma zonal
3 Ma_AtlZSST	3 Ma	3 Ma zonal
3 Ma PIZSST	3 Ma zonal	3 Ma

ture proxies (multivariate analysis of fossil planktonic foraminifera, ostracods, and diatoms as well as Mg/Ca and alkenone unsaturation index palaeothermometry) which provide greater overall confidence in the SST fields. The new multiple proxy SST estimates are now greatly enhance and extend the PRISM SST reconstruction into regions previously not represented.

2.3 Experimental design

a. 3 Ma experiments and sensitivity experiments

The fundamental framework for the control run (hereafter, 0 Ma) and the mid-Pliocene simulation (3 Ma) in this study is based on an "alternate experiment" in the PlioMIP, in which changes in land/sea are set to default values, as detailed in Haywood et al. (2010). The experiment in atmospheric composition and external forcings in this study are summarized in Table 1. The orbital configuration is specified as the same as 0 Ma setting. The concentration of CO_2 in the atmosphere was set to 280 and 405 ppmv in 0 Ma and 3 Ma. Note that the setting of atmospheric CO_2 concentration is not greatly important because the prescribed SST already includes surface warming through change in CO_2 concentrations for this study. In the absence of any adequate proxy data, all other trace gases were specified to pre-industrial value, as was the solar constant. The details of the experimental framework are described in Haywood et al. (2010).

Table 2 shows details of seven experiments conducted in this study. The surface conditions of 0 Ma and 3 Ma experiments are adjusted according to the PRISM3 datasets. The other five sensitivity experiments are designed to investigate the contributions of sea surface temperature, sea ice, topography, land ice, and vegetation to the mid-Pliocene climate. The effects of boundary parameters are evaluated in the difference between the results of the 3 Ma control experiment and

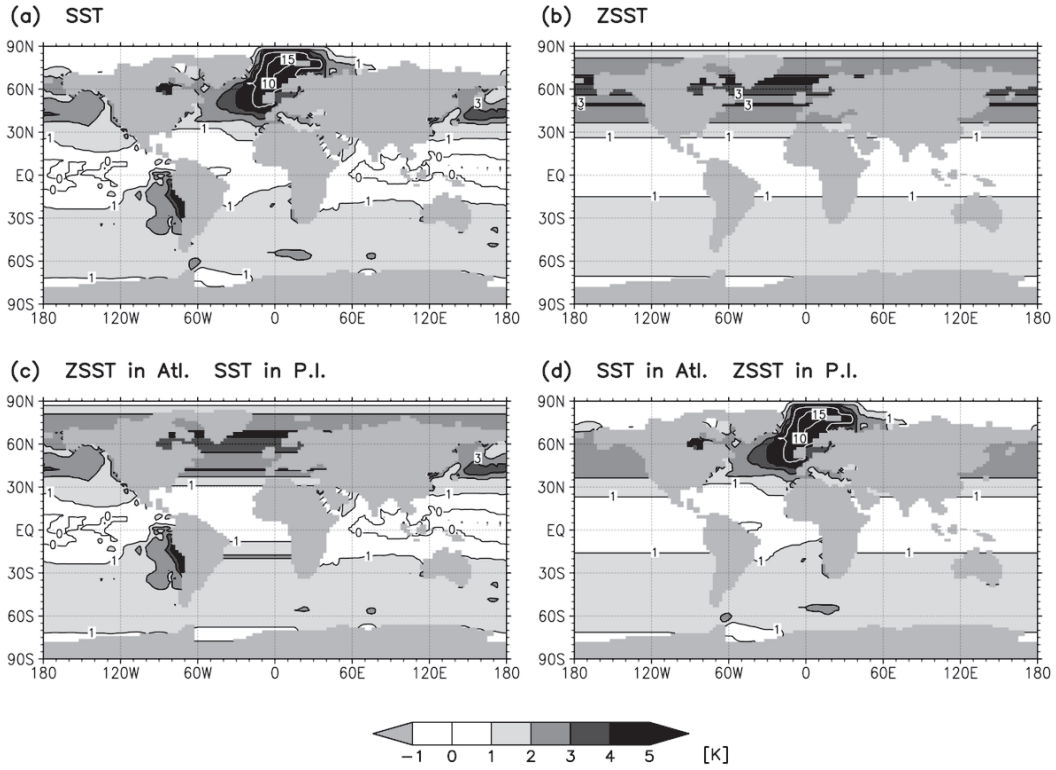

Fig. 3. Differences in annual mean SST (K) between idealized SST experiments and 0 Ma (a) 3 Ma (same as Fig. 1a), (b) 3 Ma_ZSST (zonal-mean SST in globe), (c) 3 Ma_AtlZSST (same as Fig. 3b, but for zonal SST in the Atlantic Ocean), (d) 3 Ma_PIZSST (same as Fig. 3b, but for zonal SST in the Pacific/Indian Ocean). Boundaries between the Southern Atlantic Ocean and the Southern Pacific/Indian Ocean (22.5°E, 67.5°W) are smoothed with neighboring grids.

3 Ma simulation forced by prescribed 0 Ma parameters in this study. For example, the effect of SST is calculated by subtracting the result of 3 Ma_0SST from that of 3 Ma. The basic framework for evaluating the effects of boundary conditions by sensitivity experiments is almost identical to Ueda et al. (2011). All simulations were run for 60 years, and the results reported below are climatological mean for the last 50 years.

b. Idealized SST experiments

In addition to the sensitivity simulations, we performed three additional idealized experiments, summarized in Table 3, to investigate more details in the relationship between SST distribution and 3 Ma climate. Figure 3 shows the distributions of SST anomaly in boundary conditions within the three simulations. Other boundary conditions in the experiments are similar to the 3 Ma simulation. The pattern of SST represented in Fig. 3a is the difference in SST between 3 Ma and 0 Ma boundary conditions (also shown in Fig. 1a). Figure 3b shows the pattern of zonal-mean SST anomaly between 3 Ma and 0 Ma (hereafter, ZSST). By use of ZSST, we performed "3 Ma_ZSST" simulation to separate contributions of meridional distribution in ZSST and the zonal asymmetry difference in SST between 3 Ma and 0 Ma (hereafter, ZASST). The effect of ZSST is determined by subtracting the results of the 3 Ma_ZSST from the results of the 3 Ma_0SST. Figures 3c and 3d shows the difference of SST between 3 Ma and 0 Ma, except for ZSST in the Atlantic Ocean and the Arctic Ocean (AtlZSST), and the Pacific Ocean and the Indian Ocean (PIZSST), respectively. By use of AtlZSST (PIZSST) for boundary condition, 3 Ma_AtlZSST (3 Ma_PIZSST) experiment is performed to evaluate the effect of ZASST in the Pacific Ocean and the Indian Ocean (the Atlantic Ocean) in comparison with the results of 3 Ma_ZSST. Note that the zonal-mean SST anomaly in a part of the global ocean is computed by averaging within the region (not

global) to keep meridional distribution of zonal-mean SST withthe 3 Ma simulation (Fig. 3b).

2.4 Indices of Hadley and Walker circulation

As a simple parameter to gauge the intensity of the Hadley circulation, we use the mass stream function (Oort and Yienger 1996) to represent the strength of the mean meridional overturning of mass. This index is defined by calculating the northward mass flux above a particular pressure level, p. The mass stream function of the MMC Ψ_M is defined as

$$\Psi_M = \frac{2\pi a \cos\phi}{g} \int_0^p [v] dp \tag{1}$$

where π is a circular constant, a is the radius of the earth, ϕ is the latitude, g is the gravity acceleration, and v is the meridional velocity. The operator [ ] stands for the zonal averaging. The Hadley circulation is described by two cells (Northern and Southern) of Ψ_M in the tropics. The latitudinal extent and centers of the Hadley cells are represented by the absolute value of Ψ_M at 500 hPa at zero and maximum. This index representing the intensity and width of the Hadley circulation was also used in many other studies investigating past, present and future climate changes (e.g., Kitoh and Murakami 2002; Lu et al. 2007; Ohba and Ueda 2010). The Walker circulation is calculated by the divergent component of the zonal wind in the tropics (Yu and Boer 2002; Yu and Zwiers 2010). We define a function Ψ_Z as

$$\Psi_Z = \frac{2\pi a}{g} \int_0^p u_D dp \tag{2}$$

where u_D is the averaging value of the divergent component of the zonal wind in low latitude (30°S–30°N). The two indices enable us to describe the differences in the planetary scale circulations between the mid-Pliocene and the present day.

3. Atmospheric circulation and wetter subtropics in the mid-Pliocene

3.1 Precipitation pattern

The primary feature of atmospheric circulation in the mid-Pliocene is found in meridional contrast. Figure 4 shows the annual-mean differences in surface temperature and precipitation between 3 Ma and 0 Ma simulations. The surface temperature in 3 Ma tends to be higher than 0 Ma in most parts of the globe, with a 2.1 K warming in global averaging value. Significant warming is evident in mid- and high-latitude in both hemispheres (Fig. 4a). The most prominent warming occurred in high-latitude North Atlantic, about 16 K compared to the present day. Over the ocean, the surface warming pattern bears considerable resemblance to the distribution of SST changes (Fig. 1a). The increases in the surface temperature in high latitudes correspond with the area where sea ice and land ice markedly reduced (Fig. 2). In contrast, any substantial changes are not evident in low latitude, except over the tropical eastern Pacific and subtropical North Africa. The east–west gradient in SST over the tropical Pacific was weakened remarkably (~ -4 K) because of the increasing (~ 4 K) /unchanged (~ 0 K) SST contrast over the tropical eastern/western Pacific (Fig. 1a). The surface cooling over subtropical North Africa is attributed to increase in evaporative cooling corresponding with intensification of the hydrological cycle in that region (Fig. 4d).

The precipitation pattern in low latitudes is characterized with decreasing (increasing) on the inside (outside) of the tropical rainfall zone (the area where annual-mean rainfall exceeds 4 mm day^{-1}) in 0 Ma (Fig. 4d). For example, precipitation decreases over the tropical Indian Ocean, tropical western Pacific, the equatorial central Pacific, the central South Pacific and the equatorial western Atlantic, and increases over the tropical and subtropical Africa, the Arabian Peninsula, the subtropical South Asia and subtropical Oceania. These patterns reveal that the inter-tropical convergence zone (ITCZ) in 3 Ma is broader and the rainfall accompanying large-scale convergence in ITCZ is weakened compared to 0 Ma. Although within the tropical rainfall zone, precipitation also increases over the tropical eastern Pacific and northern South America. The meridional pattern in zonal-mean precipitation anomaly (Fig. 4e) displays the rainfall reduction in the center of the ITCZ and rise in the subtropics, indicating meridional expansion of the convergence zone in low latitude. The precipitation pattern in low latitude (30°S–30°N) also represents systematical difference between 3 Ma and 0 Ma (Fig. 4f), i.e., increasing at 20°W–70°E (in the western Atlantic, the African continent, and the western Indian Ocean) and 120°W–60°W (in the eastern Pacific and the South America), and decreasing at 80°E–110°E (in the central-eastern Indian Ocean and Maritime Continent) and 140°E–150°W (in the western-central Pacific). On the outside (inside) of the convergence regions in the tropics, the 3 Ma climate is more rainy (arid) compared to 0 Ma. It is also noteworthy that the simulated wetter conditions in the subtropical regions, especially in Africa and Australia, are consistent with the paleoenvironmental reconstructions by the fossil pollen and plant macrofossil evidences (Salzmann et al. 2008).

In order to quantify the change of large-scale cir-

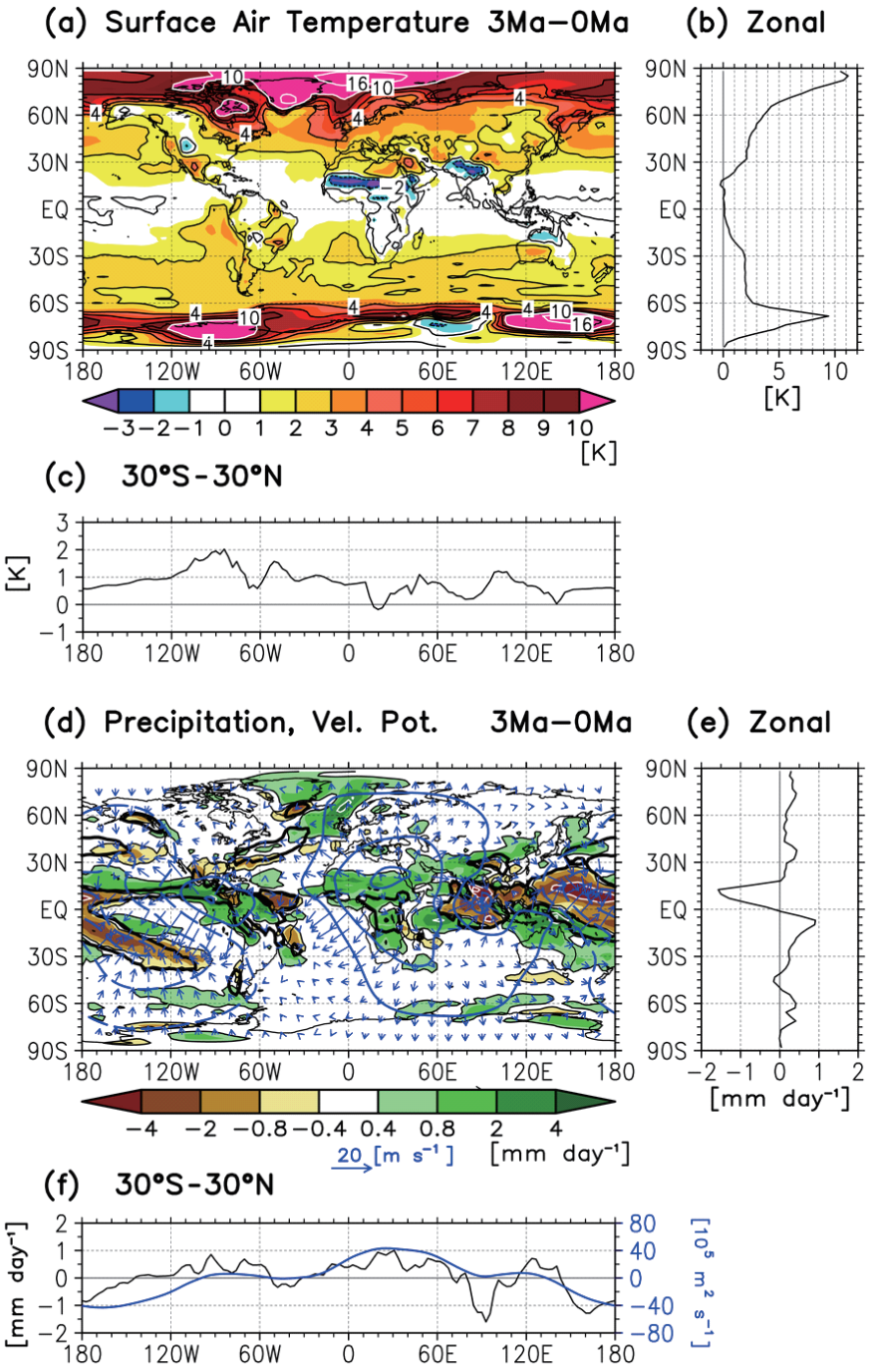

Fig. 4. Differences in the annual mean value between 3 Ma and 0 Ma. (a) Surface air temperature (K). Black and white contour interval is 2, 6 K, respectively. (b) Zonal mean of surface air temperature anomaly. (c) Low latitude (30°S–30°N) surface air temperature anomaly. (d) Precipitation (color shading in mm day^{-1}), velocity potential at 200 hPa (blue contour in 10^5 m^2 s^{-1}), and divergent wind at 200 hPa (blue vector in m s^{-1}). The thin black contour represents ±0.8, ±2 mm day^{-1} and the white contour interval is 4 mm day^{-1} in precipitation change. Solid black contour represents 4 mm day^{-1} in 0 Ma precipitation. (e) Zonal mean of precipitation anomaly. (f) Low latitude (30°S–30°N) precipitation (black line, mm day^{-1}) and velocity potential at 200 hPa (blue line, 10^5 m^2 s^{-1}) anomaly.

culation in the mid-Pliocene, velocity potential χ is used in this study. The velocity potential field is calculated using the non-rotational horizontal wind vector V_χ at 200 hPa following the definition by Krishnamurti (1971) as:

$$V_\chi = -\nabla\chi \tag{3}$$

The change of the velocity potential field in 3 Ma relative to 0 Ma is shown in Fig. 4d. The general pattern of velocity potential in 3 Ma shows that the anomalous divergent wind flows from the ITCZ to the outside regions in low latitude. The velocity potential is weakened over the western tropical Pacific and the eastern Indian Ocean where the major centers of divergent circulation, imply rising motion in the region, are located in 0 Ma (not shown). In contrast, the velocity potential in 3 Ma is strengthen over Africa, the eastern Atlantic, the western Indian Ocean, and the eastern tropical Pacific where the convergence of divergent circulation is dominated in 0 Ma. The east-west pattern of velocity potential in low latitude (Fig. 4f) is similar to that of the precipitation in low latitude. The area of the divergent/convergent anomaly in low latitude corresponds to the large-scale change of the increasing precipitation pattern at 20°W–70°E (over Africa and the western Indian Ocean) and the decreasing at 140°E–150°W (over the western-central Pacific). The changes in velocity potential over the other regions (the eastern Pacific, northern South America, the western Atlantic, and the central-eastern Indian Ocean) are near zero and the precipitation changes show complexity in latitudinal structure in low latitude.

The characteristics of atmospheric circulation and hydrological cycle in 3 Ma can be approximated by the sum of contributions of each boundary condition. Figure 5 shows the precipitation pattern in the 3 Ma simulation and the effects of the boundary conditions by the sensitivity experiments (see Section 2.3a). The precipitation change in 3 Ma (Figs. 4d and 5a) can generally be explained by the contribution of SST (Fig. 5b). As for the other boundary conditions, sea ice, topography, land ice, and vegetation (Figs. 5c–f), the contributions to the precipitation pattern in 3 Ma are negligible. Only the vegetation effect (Fig. 5f) appears as a result of the precipitation increase in subtropical North Africa and the Arabian Peninsula. The enhanced precipitation in the regions are attributed to a decrease in surface albedo and strengthening of atmospheric radiative heating, resulting in favoring convection and increased precipitation as a result of replacing forest and grassland from the current desert in those regions (e.g., Charney 1975).

The general changes in atmospheric circulation and the hydrological cycle in low latitude can largely be explained by the SST pattern in 3 Ma. Further details in the relationship between the SST distribution and 3 Ma climate are investigated by the three additional idealized experiments (see Section 2.3b). Each simulation is performed to isolate the contribution of ZSST and ZASST in each ocean sector. Figure 6 shows effect of each anomalous SST pattern on precipitation. The effect of global SST (Figs. 5b and 6a), similar to the pattern of 3 Ma simulation (Fig. 5a), shows some disagreements with pattern of ZSST (Fig. 6b). The pattern of increasing in the equatorial eastern Pacific, northern South America, and Africa, and decreasing in the central South Pacific is not evident as an effect of ZSST. The contribution of ZSST is responsible for the latitudinal characteristics of the hydrological cycle, while ZSST does little to modify the zonal asymmetry in precipitation change. In contrast, the simulation forced by 3 Ma SST in the Pacific Ocean and the Indian Ocean, as well as ZSST in the Atlantic (Fig. 3c), accurately reproduces the precipitation pattern in 3 Ma (Fig. 6a and 6c). The results of the simulation (Fig. 6d) forced by 3 Ma SST in the Atlantic Ocean and ZSST in the Pacific Ocean and the Indian Ocean (Fig. 3d) are not similar to the 3 Ma pattern (Fig. 6a). These results explain that ZASST in the Pacific Ocean and the Indian Ocean (Fig. 3c) plays a fundamental role in the zonal asymmetry of precipitation for 3 Ma.

Figure 7 shows changes in the velocity potential at 200 hPa in the idealized SST experiments. The SST effect (Fig. 7a) reproduced the altered patterns in 3 Ma very well, in addition to the precipitation change (Fig. 4d). The effect of SST is evident in the increase in divergent circulation over the eastern Atlantic, Africa, the western Indian Ocean, the eastern tropical Pacific, and northern South America, and the decreasing over the western-central Pacific. The anomalous divergent wind in 3 Ma flows from Africa and northern South America to the major divergent regions in 0 Ma (the eastern Indian Ocean and the Pacific ITCZ). Note that the major divergence over the Bay of Bengal and the eastern Indian Ocean in 0 Ma, which represents the intensity of the Asian monsoon, is attenuated in 3 Ma. The divergent anomaly over the eastern Atlantic and Africa at the upper level corresponds with weakening of the subtropical anticyclone over the Atlantic and Africa at the lower level (not shown). The contribution of ZSST for the divergent wind in 3 Ma is also seen over the eastern Indian Ocean and the western Pacific, but very restricted in strength and spatial range (Fig. 7b). As for the effect of ZASST in the Pacific/Indian Ocean (Fig. 7c) and ZASST in the Atlantic Ocean (Fig. 7d), the former contributes to the pattern

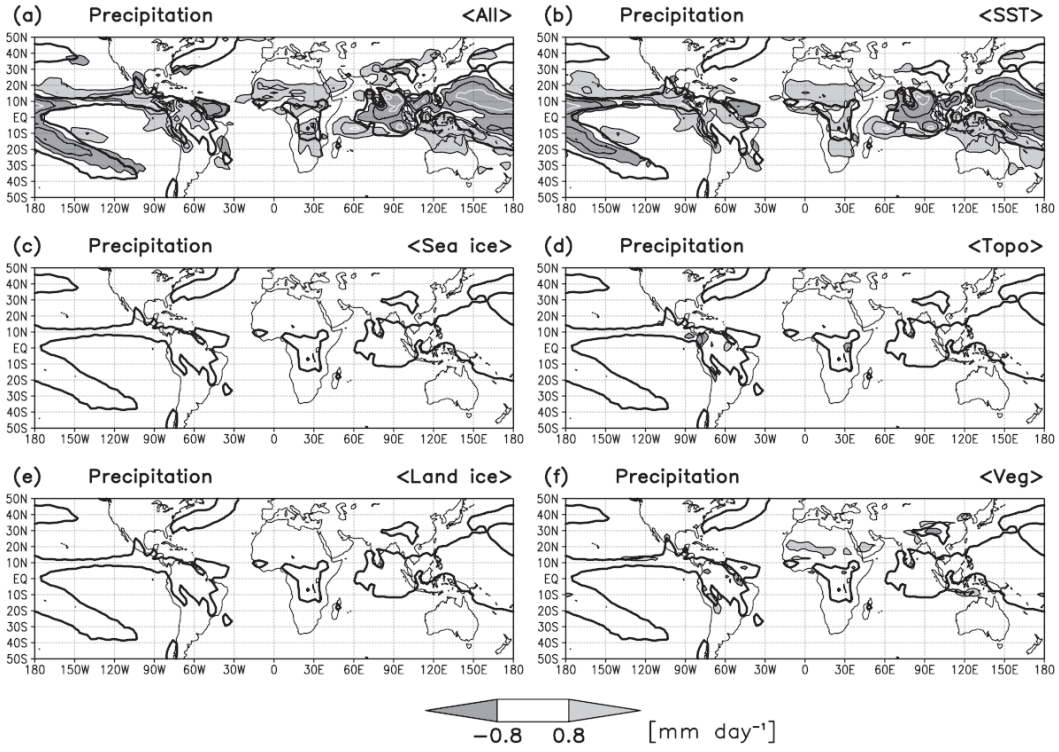

Fig. 5. Changes in the annual mean precipitation (mm day^{-1}). (a) Difference between 3 Ma and 0 Ma (same as Fig. 4d). (b) Effect of SST, (c) sea ice, (d) topography, (e) land ice, (f) vegetation. Thin black contour represents ± 0.8, ± 2 mm day^{-1}, white contour interval is 4 mm day^{-1} with the zero contours omitted for clarity. Solid black contour represents 4 mm day^{-1} in climatological value in 0 Ma.

of the SST (Fig. 7a) rather than the latter. The results explain that the changes of the meridional precipitation pattern in 3 Ma are altered by the change of the meridional gradient in SST, while the precipitation pattern in low latitude and the anomalous convergent/divergent circulations at the upper level result from the ZASST in the Pacific Ocean and Indian Ocean in 3 Ma.

3.2 Hadley and Walker circulation

The results of changes in atmospheric circulation patterns, shown in the above, imply the existence of general modification of atmospheric overturning circulation in the mid-Pliocene relative to the present day. Figure 8 shows zonal-mean atmospheric meridional circulation (e.g., Hadley circulation in the tropics) and east-west overturning circulation in low latitude (Walker circulation), defined by Eqs. (1) and (2). Increasing (decreasing) values over the negative (positive) circulation in 0 Ma climatology represent a slow-down of circulation in 3 Ma. The Hadley circulation (Figs. 8a, c) weakens (up to $\sim$30 %) in the center of regions with pronounced, deep convection (10°S–15°N) in the tropics. As for the poleward boundaries of the Hadley cells around 30°S and 30°N, the circulations are strengthened, indicating poleward widening of the Hadley cells. A more evident tendency of latitudinal expansion appeared in the ascending branches in the Hadley circulation, defined as the range between the equator boundary and center of circulation at a 500 hPa constant-pressure surface (Fig. 8c). The width of the ascending branches in the northern and southern cells in 0 Ma (3 Ma) are 7.9° (8.9°) and 19.7° (21.5°) latitude, respectively. The ascending branches in the northern and southern cells extend by about 1.0° and 1.8° latitude in 3 Ma relative to 0 Ma. Both of these expansions are much larger than the interannual variability in 0 Ma (0.3° and 0.9° latitude in the northern and the southern cells, respectively). The weakening of upward motion together with the broadening of ascending branches in the Hadley circulation is concurrent with the expansion of the tropical

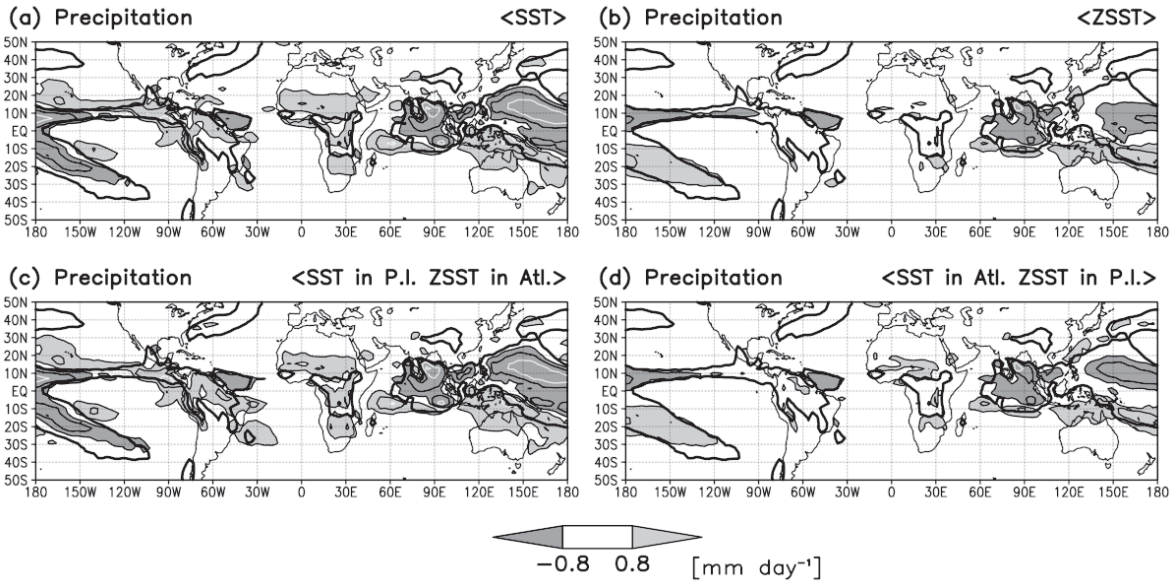

Fig. 6. Same as Fig. 5, but for the idealized SST experiments. (a) Effect of 3 Ma SST in the globe (3 Ma minus 3 Ma_0SST, same as Fig. 5b). (b) Effect of 3 Ma zonal-mean SST (ZSST) in the globe (3 Ma_ZSST minus 3 Ma_0SST). (c) Effect of 3 Ma SST in the Pacific/Indian Ocean and ZSST in the Atlantic Ocean (3 Ma_AtlZSST minus 3 Ma_0SST). (d) Effect of 3 Ma SST in the Atlantic Ocean and ZSST in the Pacific/Indian Ocean (3 Ma_PIZSST minus 3 Ma_0SST).

rainfall zone and the precipitation decrease within the area (Fig. 4e).

Figure 8b shows the Walker circulation defined by the east-west component of divergent wind integrating vertically in low latitude (Eq. 2). The annual-mean Walker circulation is represented by three major components (e.g., Hastenrath 1991; Peixoto and Oort 1992) in this study: 1) a cell ascending in the tropical western-central Pacific and descending in the eastern Pacific (Pacific Ocean cell), 2) ascending in the maritime continent, and descending in the western Indian Ocean (Indian Ocean cell), and 3) ascending in the African continent and descending in the western Atlantic (Atlantic Ocean cell). In the simulation, the Atlantic Ocean cell is represented unclearly because of conjunction of the east-west overturning circulation over South America, Atlantic, and Africa in low latitude. Boundaries between the two cells over the Indian Ocean and the Atlantic Ocean are not apparent because they merge over the western Indian Ocean. The zonally-asymmetric overturning circulations are generally weakening in 3 Ma, especially in the Pacific Ocean cell (up to $\sim$30 %) and the Indian Ocean cell (up to $\sim$66 %). The weakening of the Walker cells is attributed to the diminishing of east-west SST contrast in the tropics (Fig. 1a). The characteristics of east-west overturning circulation in 3 Ma are highly correlated with the precipitation changes in low latitude (Figs. 4d, f). The slow-down of the ascending motion between the centers of the weakened Indian Ocean cell and Pacific Ocean cell (40°E–160°W) corresponds with the attenuated precipitation area in the tropical eastern Indian Ocean and tropical western-central Pacific. In addition, the area where precipitation increases in the tropical eastern Pacific and the African continent is located in the area between the centers of the weakening cells (160°W–40°E) where large-scale descending motion is suppressed.

Figure 9 shows longitudinal distribution of velocity potential at 200 hPa in low latitude (30°S–30°N) within the idealized SST experiments. The anomalous east-west divergent contrast in 3 Ma (divergent at 20°W–70°E and convergent at 140°E–150°W) corresponds with the weakening of the Indian Walker cell and the Pacific Walker cell (Fig. 8b). The divergent anomaly over Africa and the convergent anomaly over the western-central Pacific are not sufficiently reproduced by ZSST and ZASST in the Atlantic Ocean, but it is shown by ZASST in the Pacific Ocean and the Indian

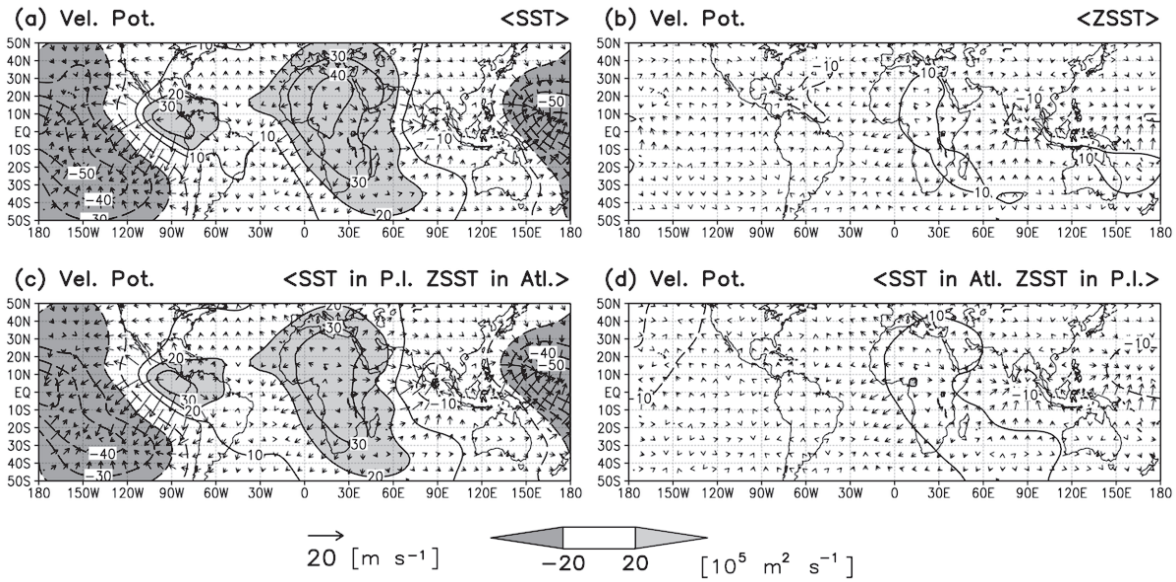

Fig. 7. Same as Fig. 6, but for velocity potential (shading and contour in 10^5 m^2 s^{-1}) and divergent wind (vector in m s^{-1}) at 200 hPa. Contour interval is 10×10^5 m^2 s^{-1} with the zero contours omitted for clarity. Solid (dashed) contour represents positive (negative) change.

Ocean, as shown in Fig. 7. These results are consistent with the fact that the amplitude of ZASST in the Pacific Ocean is much greater (∼4.0 K) than in the Indian Ocean (∼0.5 K) and in the Atlantic Ocean (∼0.5 K). The idealized experiment above reveals that the major factor contributing to the weakening of the Walker circulation over the Indian Ocean and Pacific Ocean accompanied by the zonal asymmetric changes of precipitation in 3 Ma is ZASST.

The atmospheric meridional circulation in low latitude is closely correlated to the change in the meridional gradient of SST. Figure 10 shows the changes in latitudinal range for the ascending branch in the Hadley circulation simulated by the idealized SST experiments. All of the latitudinal distributions of zonal-mean SST in the simulations (3 Ma, 3 Ma_ZSST, 3 Ma_AtlZSST, and 3 Ma_PIZSST) are the mid-Pliocene pattern. The Hadley cells in both hemispheres are expanded in the simulations by using SST with the 3 Ma latitudinal distributions of zonal-mean value. The broadening in the southern cell is larger than that in northern cell in each simulation. The extension is largest in the simulation forced by global ZSST (1.3° and 2.4° latitude in the northern and the southern cells, respectively). In either case, the broadening of the ascending branches in the Hadley cells are larger than interannual variability in the 0 Ma simulation. This result reveals that the latitudinal range of the ascending branch in the Hadley cells expands in response to the weakening of the meridional gradient of SST in 3 Ma, either zonally uniform or non-uniform.

4. Discussions

4.1 Wetter climate in subtropical Africa

In this study, the wetter surface conditions in subtropical Africa during the mid-Pliocene is also suggested by the fossil pollen data. Plio-Pleistocene climate change and the onset of aridity in the subtropics (e.g., deMenocal 1995; McLaren and Wallace 2010) had an essential role in the transition of regional paleoenvironmental conditions and the evolution of flora and fauna, including Hominids. The climate of subtropical North Africa gradually shifted from wetter to dryer conditions in the late Cenozoic (e.g., Axelrod and Raven 1978; Leroy and Dupont 1994), and begun to vary between dry and humid climates during the glacial-interglacial cycle corresponding to the fluctuation of summer insolation in the Northern Hemisphere high latitudes (e.g., Prell and Kutzbach 1987), the northern glaciations, and the cooler North Atlantic SST (e.g., deMenocal and Rind 1993; deMenocal et al. 2000). The wetter conditions in subtropical Africa and Australia (Fig. 4d) reproduced in

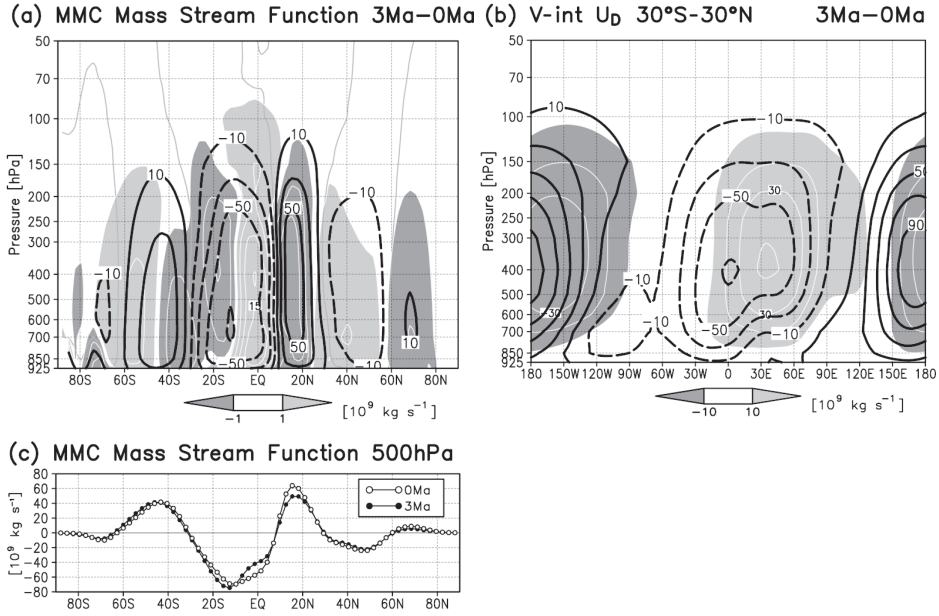

Fig. 8. (a) Mass stream function (10^9 kg s^{-1}) of the annually averaged mean meridional circulation (MMC). Black and grey contour represents climatological value in 0 Ma (black contour interval is 20×10^9 kg s^{-1}, grey contour is 0 kg s^{-1}). Shading and white contour represents the difference between 3 Ma and 0 Ma. Contour interval is 5×10^9 kg s^{-1}. (b) Vertically integrated east-west component of annual-mean divergent wind averaged over 30°S–30°N (10^9 kg s^{-1}). Black contour represents climatological value in 0 Ma. Contour interval is 20×10^9 kg s^{-1}. Shading and white contour represents the difference between 3 Ma and 0 Ma. Contour interval is 10×10^9 kg s^{-1}. (c) Latitudinal cross section of the MMC mass stream function (10^9 kg s^{-1}) at 500 hPa in 0 Ma (open circle) and 3 Ma (filled circle).

this study are mainly contributed by the pattern of SST, rather than orography, land ice, sea ice, and vegetation in this interval (Fig. 5,) through the alternation of the atmospheric circulation pattern (Fig. 7) associated with expansion of the ascending branch of Hadley circulation (Figs. 8a, c, and 10) and the slow-down of Walker circulation (Figs. 8b and 9). This study represents the importance of the diminishing in the meridional and zonal SST gradient in low latitude for the moist climate in subtropical Africa during the mid-Pliocene greenhouse world.

4.2 *Differences in the atmospheric structure with global warming projection*

The meridional-vertical structure of the tropical atmosphere is a key factor for interpreting the modulation of the atmospheric circulation (e.g., Held and Soden 2006) and climate feedback system (e.g., Soden and Held 2006) under the projected warmer conditions. Although the mid-Pliocene climate is often cited as an analog for the warmer climate, the characteristics in

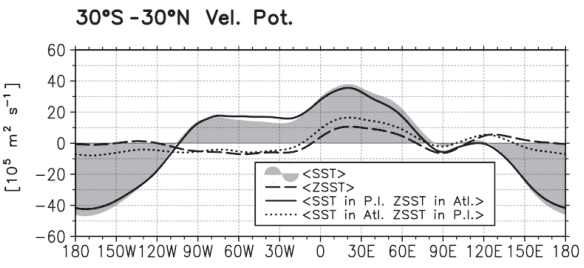

Fig. 9. Low latitude (30°S–30°N) annual mean velocity potential at 200 hPa (10^5 m^2 s^{-1}). Shading is the effect of 3 Ma SST on the globe. Dashed line is the effect of ZSST on the globe. Solid line is the effect of 3 Ma SST in the Pacific/Indian Ocean and ZSST in the Atlantic Ocean. Dotted line is the effect of 3 Ma SST in the Atlantic Ocean and ZSST in the Pacific/Indian Ocean.

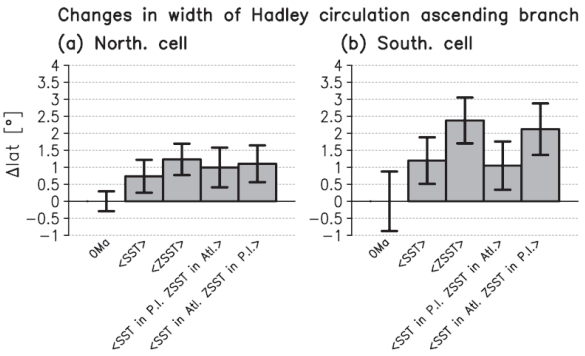

Fig. 10. Changes in latitudinal range (°) of the Hadley circulation ascending branch. Positive (negative) value represents expanding (shrinking) of the range. (a) Northern cell, (b) southern cell. Error bars indicate standard deviations in each run.

the simulation of atmospheric circulation show several differences to those of future projections. Figure 11 shows the latitude-vertical cross section of zonal-mean air temperature and specific humidity. Low- and mid-tropospheric air temperatures in 3 Ma rise significantly in mid- and high-latitude, and change slightly in low latitude (Fig. 11a). The peaks of atmospheric warming in the troposphere (∼8 K) are mainly found at near surface in high latitude regions. This pattern is different from the projected climate change forced by the increase of atmospheric greenhouse gas concentrations in which the peaks appear in the upper-troposphere in low latitude corresponding with the intensification of condensational heating (e.g., Meehl et al. 2007; Lu et al. 2008). Note that the tropical precipitation in the 3 Ma simulation does not increase relative to 0 Ma (Fig. 4e). Contrasting with the troposphere, temperatures in the stratosphere rise in the tropics and fall in mid- and high-latitudes in 3 Ma simulation. In the CO_2-rich climate, Manabe and Wetherald (1967) revealed that intensification of radiative cooling leads to temperature drop in the stratosphere by use of a one-dimensional radiative-convective equilibrium model. The stratospheric cooling simulated in the 3 Ma experiment is attributed to the rise of CO_2 concentrations in the atmosphere (Table 1). The latitudinal contrast is also evident in the zonal-mean specific humidity (Fig. 11b). The specific humidity increases in the lower troposphere, corresponding to the near-surface warming, and decreases in the lower and mid-troposphere over the equatorial region. This represents weakening of atmospheric upward motion and vertical transport of water vapor in the tropics. The atmospheric moisture pattern is accompanied with the decrease (increase) of precipitation inside (outside) the tropical rain band (Figs. 4d, e).

The weakening of atmospheric upward motion in the tropics also affects atmospheric vertical structure in the upper troposphere. Figure 12 shows tropopause height in 0 Ma and 3 Ma, calculated by the algorithm of Reichler et al. (2003) and the World Meteorological Organization (1957) (Lu et al. 2007). In low latitude, the tropopause moves downward (∼5 hPa) in 3 Ma compared to 0 Ma, and in contrast to the upward shift in the future warming simulation (Lu et al. 2008). The downward shift of the tropopause in the tropics corresponds with the weakening of atmospheric upward motion, resulting in stratospheric cooling (Fig. 11a) because atmospheric temperature begins to decrease above the tropopause level. The tropopause height outside of the tropics shifts upward, indicating poleward broadening in the characteristics of the tropical climate. The general figure of the surface conditions reconstructed by the proxy is similar to that of the global warming simulations in the aspects of mid- and high-latitude warming and El-Niño like pattern in the tropics. This work, however, shows that the zonal-mean structure of the 3 Ma atmosphere in low latitude differs from that in the future projection.

4.3 Limitations of discussions—SST formation in the mid-Pliocene

It should be noted that formation processes of the tropical SST pattern during the mid-Pliocene warm period were not discussed in this study because the results were derived from the AGCM experiments prescribing the sea-surface conditions (see Section 2.3a). Many studies have tried to improve the interpretation as to the formation and maintenance of the SST pattern in the pre-Quaternary through high latitude (ice-albedo feedback and thermohaline circulation; e.g., Crowley 1996; Robinson 2009; Etourneau et al. 2010; Steph et al. 2010) and tropical (air-sea interaction and ocean upwelling) perspectives (e.g., Philander and Fedorov 2003; Fedorov et al. 2006; Ravelo 2010). Recently, it is also found that ocean vertical mixing by tropical cyclone activities in the warmer world has an important role in the SST pattern during the early Pliocene (Fedorov et al. 2010). Further effort in improving the understanding of the control factors for mid-Pliocene sea-surface condition could benefit the prediction of climate in the future greenhouse world.

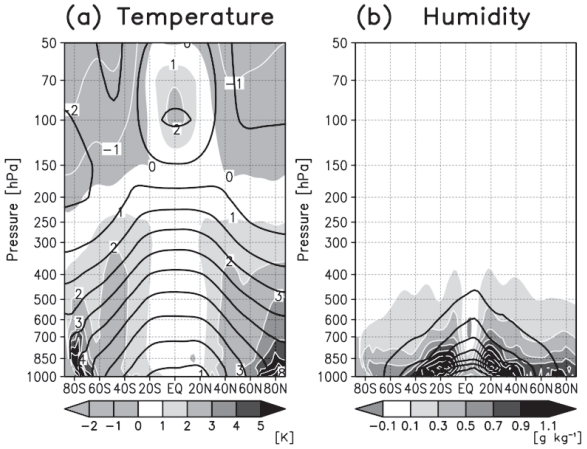

Fig. 11. Zonal average of annual mean (a) air temperature (K), (b) specific humidity (g kg^{-1}). Black contour represents climatological value in 0 Ma, shading and white contour represents the difference between 3 Ma and 0 Ma. Black and white contour interval is (a) 10, 1 K, (b) 2, 0.2 g kg^{-1}, respectively.

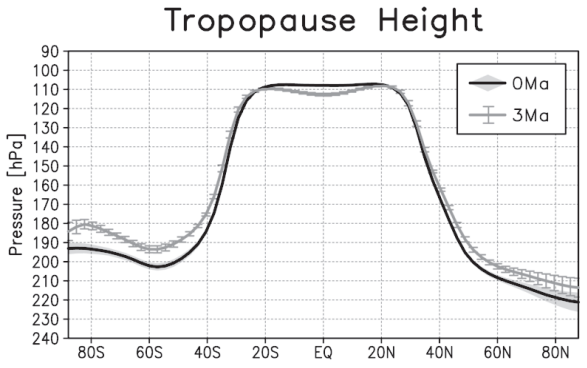

Fig. 12. Zonal average of the annual mean tropopause height (hPa). Black and grey lines represent 0 Ma and 3 Ma, respectively. Grey shading and error bars represent the range of standard deviation in 0 Ma and 3 Ma, respectively.

5. Concluding remarks

The recent improvement of SST reconstruction obtained the new proxy records, particularly in the tropical Pacific, which made significant advancement in the reproduction of atmospheric circulation patterns in the mid-Pliocene. The PRISM3 boundary condition contained the detailed information about east-west contrast in tropical oceans used in this study to enable us to describe a more systematical pattern in the atmospheric circulation. The weakening of the meridional gradient in SST suppresses the intensity of Hadley circulation and broadens the ascending branches of the Hadley cells. The expansion of the ascending area in low latitude produces wetter climate to wider regions, including subtropical Africa and Australia. The weakening of the east-west gradient of SST in the tropics, particularly in the Pacific Ocean and the Indian Ocean, corresponds with the slow-down of Walker circulation and modifies the precipitation pattern in low latitude. Further effort in the improvement of SST reconstruction during the mid-Pliocene in the tropics may help investigate the detailed aspects of sustained warmer climate.

The warm climate for a sustained time period (∼300 thousand years) is compared to present day conditions in this study. The mid-Pliocene climate was also perturbed corresponding with the fluctuation in orbital configuration, amplifying the interactions between climate subsystems (e.g., Philander and Fedorov 2003; Fedorov et al. 2006) or closure of Oceanic gateways (e.g., Haug and Tiedemann 1998; Bartoli et al. 2005; Lunt et al. 2008; Steph et al. 2010), and gradually shifted to the Quaternary climate. The details of the processes of transition should be investigated by GCMs coupled with Ocean and other subsystems (e.g., ice sheet and vegetation) with numerous experimental configurations. As this work focuses on the climate change in low latitude, the extent and volume of sea ice and land ice are not discussed with enough detail. However, the fluctuations in the arctic sea ice, ice sheet extent in high latitude, and intensity of Atlantic meridional overturning circulation are the hot topics for comparison with the Quaternary and future climate changes. The proxy data in high latitude North Atlantic, Arctic region, and deep sea of the Atlantic has been investigated recently (e.g., Billups et al. 1997; Knies et al. 2002; Cronin et al. 2005; Poore et al. 2006; Dowsett et al. 2009b; Robinson 2009). It may help the progress of future work researching a comprehensive figure of the mid-Pliocene climate system.

In this study, only the annual-mean values are considered in order to investigate the features of the atmospheric global circulation in the mid-Pliocene. However, the seasonal or interannual characteristics in the mid-Pliocene climate also have great significance in how the climate system in the sustained warm period is formed and maintained. Particularly, comparison of the global monsoon system between in the glacial-interglacial period and in the mid-Pliocene is one of the important remaining subjects. The attenuated precipitation over the eastern Indian Ocean and Bay of Ben-

gal, attributed to weakening of Asian summer monsoon, corresponds to the increase in subtropical North Africa and Arabian Peninsula. The precipitation pattern is suggestive of a negative monsoon-desert mechanism (Rodwell and Hoskins 1996), which is a worthwhile issue in regards to investigating the seasonal aspect of climate. More detailed studies about the modification of the West African and South African monsoon could help to capture a comprehensive image into the formation of the wetter African climate in the mid-Pliocene.

Acknowledgements

The authors would like to sincerely thank the PRISM group for providing the PRISM3 dataset. We are grateful to Drs. S. Yukimoto and O. Arakawa in the Meteorological Research Institute for technical support. We thank Dr. M. Ohba in the Central Research Institute of the Electric Power Industry and T. Inoue of the University of Tsukuba for their helpful discussion and suggestions. Part of the numerical calculation for the present work has been carried out under the "Interdisciplinary Computational Science Program" in the Center for Computational Sciences, University of Tsukuba. This work is supported by the Global Environment Research Fund (S-5-2) of the Ministry of the Environment, Japan. The authors also acknowledge the constructive comments of two anonymous reviewers.

References

Axelrod, D. I., and P. H. Raven, 1978: Late Cretaceous and Tertiary vegetation history of Africa. In *Biogeography and Ecology of Southern Africa*, Eds. Werger, M. J. A., Junk, The Hague, 77–130.

Barreiro, M., G. Philander, R. Pacanowski, and A. Fedorov, 2006: Simulations of warm tropical conditions with application to Middle Pliocene atmospheres. *Climate Dyn.*, **26**, 349–365.

Bartoli, G., M. Sarnthein, M. Weinelt, H. Erlenkeuser, D. Garbe-Schönberg, and D. W. Lea, 2005: Final closure of Panama and the onset of northern hemisphere glaciation. *Earth Planet. Sci. Lett.*, **237**, 33–44.

Billups, K., A. C. Ravelo, and J. C. Zachos, 1997: Early Pliocene deep-water circulation: stable isotope evidence for enhanced northern component deep water. *Proc. Ocean Drill. Program, Sci. Results*, **154**, 319–330.

Braconnot, P., B. Otto-Bliesner, S. Harrison, S. Joussaume, J.-Y. Peterchmitt, A., Abe-Ouchi, M. Crucifix, E. Driesschaert, Th. Fichefet, C. D. Hewitt, M. Kageyama, A. Kitoh, A. Laine, M.-F. Loutre, O. Marti, U. Merkel, G. Ramstein, P. Valdes, L. Weber, Y. Yu, and Y. Zhao, 2007a: Results of PMIP2 coupled simulations of the mid-Holocene and Last Glacial Maximum—Part 1: experiments and large-scale features. *Clim. Past*, **3**, 261–277.

Braconnot, P., B. Otto-Bliesner, S. Harrison, S. Joussaume, J.-Y. Peterchmitt, A. Abe-Ouchi, M. Crucifix, E. Driesschaert, Th. Fichefet, C. D. Hewitt, M. Kageyama, A. Kitoh, M.-F. Loutre, O. Marti, U. Merkel, G. Ramstein, P. Valdes, S. L. Weber, Y. Yu, and Y. Zhao, 2007b: Results of PMIP2 coupled simulations of the Mid-Holocene and Last Glacial Maximum—Part 2: feedbacks with emphasis on the location of the ITCZ and mid-and high latitudes heat budget. *Clim. Past*, **3**, 279–296.

Brierley, C. M., A. V. Fedorov, Z. Liu, T. D. Herbert, K. T. Lawrence, and J. P. LaRiviere, 2009: Greatly expanded tropical warm pool and weakened Hadley circulation in the early Pliocene. *Science*, **323**, 1714–1718.

Chandler, M. A., D. Rind, and R. S. Thompson, 1994: Joint investigations of the middle Pliocene climate II: GISS GCM Northern Hemisphere results. *Global Planet. Change*, **9**, 197–219.

Charney, J. G., 1975: Dynamics of deserts and drought in the Sahel. *Quart. J. Roy. Meteor. Soc.*, **101**, 193–202.

Cronin, T. M., H. J. Dowsett, G. S. Dwyer, P. A. Baker, and M. A. Chandler, 2005: Mid-Pliocene deep-sea bottom-water temperatures based on ostracode Mg/Ca ratios. *Mar. Micropaleontol.*, **54**, 249–261.

Crowley, T. J., 1996: Pliocene climates: The nature of the problem. *Mar. Micropaleontol.*, **27**, 3–12.

Dekens, P. S., A. C. Ravelo, and M. D. McCarthy, 2007: Warm upwelling regions in the Pliocene warm period. *Paleoceanography*, **22**, PA3211, doi:10.1029/2006PA001394.

deMenocal, P. B., 1995: Plio-Pleistocene African climate. *Science*, **270**, 53–59.

deMenocal, P. B., and D. Rind, 1993: Sensitivity of Asian and African climate to variations in seasonal insolation, glacial ice cover, sea surface temperature, and Asian orography. *J. Geophys. Res.*, **98**, 7265–7287.

deMenocal, P., J. Ortiz, T. Guilderson, J. Adkins, M. Sarnthein, L. Baker, and M. Yarusinsky, 2000: Abrupt onset and termination of the African Humid Period: rapid climate responses to gradual insolation forcing. *Quart. Sci. Rev.*, **19**, 347–361.

Dowsett, H. J., and M. M. Robinson, 2009: Mid-Pliocene equatorial Pacific sea surface temperature reconstruction: a multi-proxy perspective. *Phil. Trans. R. Soc. A*, **367**, 109–125.

Dowsett, H. J., R.S. Thompson, J. A. Barron, T. M. Cronin, R. F. Fleming, S. E. Ishman, R. Z. Poore, D. A. Willard, and T. R. Holtz, 1994: Joint investigations of the middle Pliocene climate I: PRISM paleoenvironmental reconstructions. *Global Planet. Change*, **9**, 169–195.

Dowsett, H., J. Barron, and R. Poore, 1996: Middle Pliocene sea surface temperatures: a global reconstruc-

tion. *Mar. Micropaleontol*., **27**, 13–26.

Dowsett, H. J., J. A. Barron, R. Z. Poore, R. S. Thompson, T. M. Cronin, S. E. Ishman, and D. A. Willard, 1999: Middle Pliocene paleoenvironmental reconstruction: PRISM2. *U.S. Geol. Surv. Open File Rep*., 99–535.

Dowsett, H. J., M. A. Chandler, and M. M. Robinson, 2009a: Surface temperatures of the Mid-Pliocene North Atlantic Ocean: implications for future climate. *Phil. Trans. R. Soc. A*, **367**, 69–84.

Dowsett, H. J., M. M. Robinson, and K. M. Foley, 2009b: Pliocene three-dimensional global ocean temperature reconstruction. *Clim. Past*, **5**, 769–783.

Etourneau, J., R. Schneidera, T. Blanza, and P. Martinez, 2010: Intensification of the Walker and Hadley atmospheric circulations during the Pliocene-Pleistocene climate transition. *Earth Planet. Sci. Lett*., **297**, 103–110.

Fedorov, A. V., P. S. Dekens, M. McCarthy, A. C. Ravelo, P. B. deMenocal, M. Barreiro, R. C. Pacanowski, and S. G. Philander, 2006: The Pliocene paradox (mechanisms for a permanent El Niño). *Science*, **312**, 1485–1489.

Fedorov, A. V., C. M. Brierley, and K. Emanuel, 2010: Tropical cyclones and permanent El Niño in the early Pliocene epoch. *Nature*, **463**, 1066–1070.

Hastenrath, S., 1991: Climate dynamics of the tropics. Kluwer Academic Publishers, Dortrecht, 488 pp.

Haug, G. H., and R. Tiedemann, 1998: Effect of the formation of the Isthmus of Panama on Atlantic Ocean thermohaline circulation. *Nature*, **393**, 673–676.

Haywood, A. M., and P. J. Valdes, 2006: Vegetation cover in a warmer world simulated using a dynamic global vegetation model for the Mid-Pliocene. *Palaeogeogr. Palaeoclimatol. Palaeoecol*., **237**, 412–427.

Haywood, A. M., P. J. Valdes, and B. W. Sellwood, 2000: Global scale palaeoclimate reconstruction of the middle Pliocene climate using the UKMO GCM: initial results. *Global Planet. Change*, **25**, 239–256.

Haywood, A. M., P. Dekens, A. C. Ravelo, and M. Williams, 2005: Warmer tropics during the mid-Pliocene? Evidence from alkenone paleothermometry and a fully coupled ocean-atmosphere GCM. *Geochem. Geophys. Geosys.*, **6**, Q03010, doi:10.1029/2004GC000799.

Haywood, A. M., H. J. Dowsett, P. J. Valdes, D. J. Lunt, J. E. Francis, and B. W. Sellwood, 2009a: Introduction. Pliocene climate, processes and problems. *Phil. Trans. R. Soc. A*, **367**, 3–17.

Haywood, A. M., M. A. Chandler, P. J. Valdes, U. Salzmann, D. J. Lunt, and H. J. Dowsett, 2009b: Comparison of mid-Pliocene climate predictions produced by the HadAM3 and GCMAM3 General Circulation Models. *Global Planet. Change*, **66**, 208–224.

Haywood, A. M., H. J. Dowsett, B. Otto-Bliesner, M. A. Chandler, A. M. Dolan, D. J. Hill, D. J. Lunt, M. M. Robinson, N. Rosenbloom, U. Salzmann, and L. E. Sohl, 2010: Pliocene Model Intercomparison Project (PlioMIP): experimental design and boundary conditions (Experiment 1). *Geosci. Model Dev*., **3**, 227–242.

Held, I. M., and B. J. Soden, 2006: Robust responses of the hydrological cycle to global warming. *J. Climate*, **19**, 5686–5699.

Jansen, E., J. Overpeck, K. R. Briffa, J.-C. Duplessy, F. Joos, V. Masson-Delmotte, D. Olago, B. Otto-Bliesner, W. R. Peltier, S. Rahmstorf, R. Ramesh, D. Raynaud, D. Rind, O. Solomina, R. Villalba, and D. Zhang, 2007: Palaeoclimate. In *Climate change 2007: the physical science basis. Contribution of working group I to the fourth assessment report of the Intergovernmental Panel on Climate Change,* Eds. S. Solomon, D. Qin, M. Manning, Z. Chen, M. Marquis, K. B. Averyt, M. Tignor, and H. L. Miller, Cambridge University Press, Cambridge, 433–498.

Jiang, D., H. Wang, Z. Ding, X. Lang, and H. Drange, 2005: Modeling the middle Pliocene climate with a global atmospheric general circulation model. *J. Geophys. Res*., **110**, D14107, doi:10.1029/2004JD005639.

Joussaume, S., K. E. Taylor , P. Braconnot, J. F. B. Mitchell, J. E. Kutzbach, S. P. Harrison, I. C. Prentice, A. J. Broccoli, A. Abe-Ouchi, P. J. Bartlein, C. Bonfils, B. Dong, J. Guiot, K. Herterich, C. D. Hewitt, D. Jolly, J. W. Kim, A. Kislov, A. Kitoh, M. F. Loutre, V. Masson, B. McAvaney, N. McFarlane, N. de Noblet, W. R. Peltier, J. Y. Peterschmitt, D. Pollard, D. Rind, J. F. Royer, M. E. Schlesinger, J. Syktus, S. Thompson, P. Valdes, G. Vettoretti, R. S. Webb, and U. Wyputta, 1999: Monsoon changes for 6000 years ago: results of 18 simulations from the Paleoclimate Modeling Intercomparison Project (PMIP). *Geophys. Res. Lett.,* **26**, 859–862.

Kitoh, A., and S. Murakami, 2002: Tropical Pacific climate at the mid-Holocene and the Last Glacial Maximum simulated by a coupled ocean-atmosphere general circulation model. *Paleoceanography*, **17**, 1047, doi:10.1029/2001PA000724.

Kitoh, A., S. Murakami, and H. Koide, 2001: A simulation of the Last Glacial Maximum with a coupled atmosphere-ocean GCM. *Geophys. Res. Lett*., **28**, 2221–2224.

Knies, J., J. Matthiessen, C. Vogt, and R. Stein, 2002: Evidence of 'Mid-Pliocene (∼3 Ma) global warmth' in the eastern Arctic Ocean and implications for the Svalbard/Barents Sea ice sheet during the late Pliocene and early Pleistocene (∼3–1.7 Ma). *Boreas*, **31**, 82–93.

Knutti, R., and G. C. Hegerl, 2008: The equilibrium sensitivity of the Earth's temperature to radiation changes. *Nature Geosci.*, **1**, 735–743.

Krishnamurti, T. N., 1971: Tropical east-west circulations during the northern summer. *J. Atmos. Sci*. **28**, 1342–1347.

Leroy, S., and L. Dupont, 1994: Development of vegetation

and continental aridity in northwestern Africa during the Late Pliocene: the pollen record of ODP site 658. *Palaeogeogr. Palaeoclimatol. Palaeoecol.*, **109**, 295–316.

Lisiecki, L. E., and M. E. Raymo, 2005: A Pliocene-Pleistocene stack of 57 globally distributed benthic δ18O records. *Paleoceanography*, **20**, PA1003, doi:10.1029/2004PA001071.

Lu, J., G. A. Vecchi, and T. Reichler, 2007: Expansion of the Hadley cell under global warming. *Geophys. Res. Lett.*, **34**, L06805, doi:10.1029/2006GL028443.

Lu, J., G. Chen, and D. M. W. Frierson, 2008: Response of the zonal mean atmospheric circulation to El Niño versus global warming. *J. Climate*, **21**, 5835–5851.

Lunt, D. J., P. J. Valdes, A. Haywood, and I. C. Rutt, 2008: Closure of the Panama Seaway during the Pliocene: implications for climate and Northern Hemisphere glaciation. *Climate Dyn.*, **30**, 1–18.

Lunt, D. J., A. M. Haywood, G. A. Schmidt, U. Salzmann, P. J. Valdes, and H. J. Dowsett, 2010: Earth system sensitivity inferred from Pliocene modelling and data. *Nature Geosci.*, **3**, 60–64.

Manabe, S., and R. T. Wetherald, 1967: Thermal equilibrium of the atmosphere with a given distribution of relative humidity. *J. Atmos. Sci.*, **24**, 241–259.

McLaren, S., and M. W. Wallace, 2010: Plio-Pleistocene climate change and the onset of aridity in southeastern Australia. *Global Planet. Change*, **71**, 55–72.

Meehl, G. A., T. F. Stocker, W. D. Collins, P. Friedlingstein, A. T. Gaye, J. M. Gregory, A. Kitoh, R. Knutti, J. M. Murphy, A. Noda, S. C. B. Raper, I. G. Watterson, A. J. Weaver, and Z.-C. Zhao, 2007: Global climate projections. In *Climate change 2007: the physical science basis. Contribution of working group I to the fourth assessment report of the Intergovernmental Panel on Climate Change,* Eds. S. Solomon, D. Qin, M. Manning, Z. Chen, M. Marquis, K. B. Averyt, M. Tignor, and H. L. Miller, Cambridge University Press, Cambridge, 747–846.

Ohba, M., and H. Ueda, 2010: A GCM study on effects of continental drift on tropical climate at the early and late Cretaceous. *J. Meteor. Soc. Japan*, **88**, 869–881.

Oort, A. H., and J. J. Yienger, 1996: Observed interannual variability in the Hadley circulation and its connection to ENSO. *J. Climate*, **9**, 2751–2767.

Otto-Bliesner, B. L., S. P. Harrison, and A. Abe-Ouchi, 2009: Modeling and data syntheses of past climates. *EOS Trans. AGU*, **90**, 93–93.

Pagani, M., Z. Liu, J. Lariviere, and A. C. Ravelo, 2010: High Earth-system climate sensitivity determined from Pliocene carbon dioxide concentrations. *Nature Geosci.*, **3**, 27–30.

Peixoto, J., and A. Oort, 1992: The physics of climate. American Institute of Physics, New York, 520 pp.

Philander, S. G., and A. V. Fedorov, 2003: Role of tropics in changing the response to Milankovich forcing some three million years ago. *Paleoceanography*, **18**, 1045, doi:10.1029/2002PA000837.

Poore, H. R., R. Samworth, N. J. White, S. M. Jones, and I. N. McCave, 2006: Neogene overflow of Northern Component Water at the Greenland-Scotland Ridge. *Geochem. Geophys. Geosyst.*, **7**, Q06010, doi:10.1029/2005GC001085.

Prell, W. L., and J. E. Kutzbach, 1987: Monsoon variability over the past 150,000 years. *J. Geophys. Res.*, **92**, 8411–8425.

Ravelo, A. C., 2010: Warmth and glaciation. *Nature Geosci.*, **3**, 672–674.

Ravelo, A. C., D. H. Andreasen, M. Lyle, A. O. Lyle, and M. W. Wara, 2004: Regional climate shifts caused by gradual global cooling in the Pliocene epoch. *Nature*, **429**, 263–267.

Reichler, T., M. Dameris, and R. Sausen, 2003: Determining the tropopause height from gridded data. *Geophys. Res. Lett.*, **30**, 2042, doi:10.1029/2003GL018240.

Robinson, M. M., 2009: New quantitative evidence of extreme warmth in the Pliocene arctic. *Stratigraphy*, **6**, 1–10.

Rodwell, M. J., and B. J. Hoskins, 1996: Monsoons and the dynamics of deserts. *Quart. J. Roy. Meteor. Soc.*, **122**, 1385–1404.

Salzmann, U., A. M. Haywood, D. J. Lunt, P. J. Valdes, and D. J. Hill, 2008: A new global biome reconstruction and data-model comparison for the Middle Pliocene. *Glob. Ecol. Biogeogr.*, **17**, 432–447.

Salzmann, U. A., M. Haywood, and D. J. Lunt, 2009: The past is a guide to the future? Comparing Middle Pliocene vegetation with predicted biome distributions for the twenty-first century. *Phil. Trans. R. Soc. A*, **367**, 189–204.

Sato, N., P. J. Sellers, D. A. Randall, E. K. Schneider, J. Shukla, J. L. Kinter, Y.-Y. Hou, and E. Albertazzi, 1989: Effects of implementing the simple biosphere model in a general circulation model. *J. Atmos. Sci.*, **46**, 2757–2782.

Sellers, P. J., Y. Mintz, Y. C. Sud, and A. Dalcher, 1986: A simple biosphere model (SiB) for use within general circulation models. *J. Atmos. Sci.*, **43**, 505–531.

Sloan, L. C., T. J. Crowley, and D. Pollard, 1996: Modeling of middle Pliocene climate with the NCAR GENESIS general circulation model. *Mar. Micropaleontol.*, **27**, 51–61.

Soden, B. J., and I. M. Held, 2006: An assessment of climate feedbacks in coupled ocean-atmosphere models. *J. Climate*, **19**, 3354–3360.

Sohl, L. E., M. A. Chandler, R. B. Schmunk, K. Mankoff, J. A. Jonas, K. M. Foley, and H. J. Dowsett, 2009: PRISM3/GISS topographic reconstruction. *U.S. Geological Survey Data Series*, **419**, 6 pp.

Steph, S., R. Tiedemann, M. Prange, J. Groeneveld, M. Schulz, A. Timmermann, D. Nürnberg, C. Rühlemann, C. Saukel, and G. H. Haug, 2010: Early Pliocene

increase in thermohaline overturning: A precondition for the development of the modern equatorial Pacific cold tongue. *Paleoceanography*, **25**, PA2202, doi:10.1029/2008PA001645.

Thompson, R. S., and R. F. Fleming, 1996: Middle Pliocene vegetation: reconstructions, paleoclimatic inferences, and boundary conditions for climate modeling. *Mar. Micropaleontol.*, **27**, 27–49.

Ueda, H., H. Kuroki, M. Ohba, and Y. Kamae, 2011: Seasonally asymmetric transition of the Asian monsoon in response to ice age boundary conditions. *Climate Dyn.*, in press.

Wara, M. W., A. C. Ravelo, and M. L. Delaney, 2005: Permanent El Niño-like conditions during the Pliocene warm period. *Science*, **309**, 758–761.

World Meteorological Organization, 1957: Meteorology - A three-dimensional science: Second session of the commission for aerology. *WMO Bull.*, **IV**, 134–138.

Yu, B., and G. J. Boer, 2002: The roles of radiation and dynamical processes in the El Niño-like response to global warming. *Climate Dyn.*, **19**, 539–553.

Yu, B., and F. W. Zwiers, 2010: Changes in equatorial atmospheric zonal circulations in recent decades. *Geophys. Res. Lett.*, **37**, L05701, doi:10.1029/2009GL042071.

Yukimoto, S., A. Noda, A. Kitoh, M. Sugi, Y. Kitamura, M. Hosaka, K. Shibata, S. Maeda, and T. Uchiyama, 2001: The new meteorological research institute coupled GCM (MRI-CGCM2)—Model climate and variability—. *Pap. Meteor. Geophys.*, **51**, 47–88.

Yukimoto, S., A. Noda, A. Kitoh, M. Hosaka, H. Yoshimura, T. Uchiyama, K. Shibata, O. Arakawa, and S. Kusunoki, 2006: Present-day and climate sensitivity in the meteorological research institute coupled GCM version 2.3 (MRI-CGCM2.3). *J. Meteor. Soc. Japan*, **84**, 333–363.

Zachos, J., M. Pagani, L. Sloan, E. Thomas, and K. Billups, 2001: Trends, rhythms, and aberrations in global climate 65 Ma to present. *Science*, **292**, 686–693.